This article has been accepted for publication in a future issue of this journal, but has not been fully edited. Content may change prior to final publication. Citation information: DOI 10.1109/JSEN.2018.2880999, IEEE Sensors Journal

An agile electrical capacitance tomography system with improved frame rates

Ang Huang, Zhang Cao*, *Member, IEEE*, Shijie Sun, *Member, IEEE*, Fanghao Lu, Lijun Xu, *Senior Member, IEEE*

多频激励测量

***Abstract*—In this paper, an AC-based agile parallel hardware system was introduced for ECT. A multi-frequency excitation and measurement strategy was proposed to minimize the switching time between different channels. For an ECT sensor with 2^m electrodes, all the mutual capacitances can be measured much faster, which is $m/(2^m-1)$ of the time used by the classical single-frequency excitation and measurement strategy. It implies that the proposed strategy accelerates the capacitance acquisition in an exponential way. Besides the efforts made to reduce the switching times between channels, the operating time of each electronic switch was selected to fasten the demodulation. The hardware fabricated here can be modified agilely by running codes, and different excitation and demodulation methods can be implemented on the chip. To verify the performance of the agile system, ECT sensors with different electrodes are facilitated to measure the mutual capacitances. The capacitances can be achieved with a frame rate of respectively up to 15.15 kilo frames per second (kfps) and 12.82 kfps in the cases of twelve and sixteen electrodes. The ignition process of a flame generated by a Bunsen burner can be captured by the proposed system. Also, the discharging of the igniter can be imaged, and it is usually undistinguishable in a low-speed system.**

***Index Terms*—Electrical capacitance tomography, multi-frequency excitation, agile hardware implementation, high frame rate, ignition process monitoring.**

I. Introduction

Electrical capacitance tomography (ECT) utilizes the mutual capacitances between different electrodes to image the permittivity distribution surrounded by the electrode array. Compared with other process imaging techniques, such as X ray tomography and ultrasonic tomography, ECT offers advantages on no radiation, non-invasiveness, rapid response, easy installation and low cost [1]. In the past decades, the ECT techniques found successful applications in the void fraction measurement and flow pattern recognition for gas-liquid two phase flow [2, 3], visualization of concentration distribution for gas-solid two-phase flow in pipelines [4, 5] and flame monitoring [6], etc. For the ECT system, once the number of electrodes in the sensor is fixed, its frame rate is mainly restricted by the switching time between different channels and the demodulation time in each channel. The switching time is determined by the number of switching between channels and the response time of each electronic switch. The demodulation time relies on the number of sampling points used for calculations.

开关时间、解调时间

In the cascade ECT system, only one excitation circuit and one current detector are used and then the mutual capacitance between every two electrodes needs to be measured one after another [7, 8]. The number of channel switching equals to the total number of the mutual capacitances, i.e. $N(N-1)/2$ for a N-electrode ECT sensor. The number can be reduced by parallelizing N-1 channels to detect the mutual capacitances simultaneously, and N-1 capacitance detection circuits were fabricated to achieve the multi-channel parallel strategy [9, 10]. In this case, the switching number is only one-(N/2)th of that in a cascade system, and the frame rate on the hardware implementation reached 1.25 kfps for a 16-electrode sensor [11, 12]. For an ECT sensor with twelve electrodes, the capacitance acquisition in a typical multi-channel parallel ECT system enabled a frame rate up to 11 kfps in our previous work[13]. However, when the frame rate reaches over 11 kfps, each electronic switch was switched within 5μs and it is too short to stabilize the measurement signals. In this case, the standard deviation of a 200 fF capacitor for one hundred repetitive measurements will overpass 4 fF, and it will severely distort the image reconstruction in ECT. Code-division multiplexing using pseudorandom sequences can also be used to reduce the switching, thereby improving the acquisition speed of hardware system. However, the quality of the measured data produced are degraded due to the lack of completely orthogonal code sets in reality [14, 15]. Another way to reduce the number is utilizing the multiple frequency for excitation and measurement [16-20]. Sinusoid excitation signals at different frequencies are simultaneously applied on different excitation electrodes and the electrical current signals on the measurement electrodes are used to detect the capacitances. Unlike the multi-channel parallel strategy at single excitation frequency, more mutual capacitances are measured at the same time [21], and the number of channel switching can be further reduced. However, the multi-frequency ECT system has not been realized on an integrated hardware system [1].

通过并行化N-1通道同时检测互电容可以减少数量，并且制造N-1电容检测电路以实现多通道并行策略

During the channel switching, the electronic switches need time to response, and the over-zero switching scheme was applied to suppress the signal fluctuation from the switching [22]. The switches are operated exactly at the zero angles of the

This work was supported from the National Natural Science Foundation of China (No. 61522102, 61871017, 61620106004), National key R & D program on Major scientific equipment development (2016YFF0100602) and Program for Changjiang Scholar and Innovative Research Team in University (IRT1203).

The authors are with department of measurement and control, School of Instrumentation and Optoelectronic Engineering and Honor College, Beihang University, Beijing 100191, China and Beijing Advanced Innovation Center for Big Data-Based Precision Medicine, Beijing 100191, China.

(*Corresponding author, e-mail: zh_cao@buaa.edu.cn)

1558-1748 (c) 2018 IEEE. Personal use is permitted, but republication/redistribution requires IEEE permission. See http://www.ieee.org/publications_standards/publications/rights/index.html for more information.

This article has been accepted for publication in a future issue of this journal, but has not been fully edited. Content may change prior to final publication. Citation information: DOI 10.1109/JSEN.2018.2880999, IEEE Sensors Journal

sinusoidal signal, and the response time can be dramatically reduced at the same precision [23]. However, the random distortions in the channel switching makes it hard to predict the instants of zero-crossing. In this case, the switches usually fail to accurately turn on and off between channels, especially if the frequency of the excitation signal or the number of excitation electrodes is increased. As a result, the intermittent excitation signals were used to achieve the hold-zero switching scheme. It eliminates the distortion from the switching fluctuation and is suitable for the multi-channel parallel systems with high excitation frequencies [24]. This scheme requires precise synchronization of several intermittent excitation signals, and dramatically complicated the hardware implementation in the ECT system.

In each channel, the capacitance acquisition rate can be improved by shortening the demodulation time [25]. In multi-frequency electrical impedance measurement, the Fast Fourier Transformation (FFT) requires sufficient sampling data [26-28], and it is not suitable for ECT systems with high temporal resolutions. The phase-sensitive demodulators, e.g. rectification demodulator[7], the digital switching demodulator [29] and the multiplication demodulator [30] can be implemented on the chip, such as a high-performance field programmable gate array (FPGA) or a digital signal processor (DSP), but its dynamic response is limited by the excitation frequency. Recursive non-integer-period demodulation methods developed in our previous work can be utilized to acquire the demodulated value with one excitation period and accelerate the demodulation [31, 32], and successful application can be found in the parallel ECT systems with single-frequency excitations [13].

In this paper, an AC-based agile multi-frequency excitation and measurement ECT hardware system was proposed. Optimal switching scheme is proposed in *section II. B* to minimize the switching number between different channels. Besides, the response time for electronic switches are compared and selected in the demodulation for the first time in *section II. C*. Instead of hold-zero switching scheme, a grounded hold-zero switching scheme is proposed to reduce the response time in each channel switching in multi-frequency ECT systems. Both classical multiplication demodulation and iterative non-integer-period demodulation was implemented in the FPGA. The capacitance acquisition rate of the proposed multi-frequency ECT system was evaluated by using a high-speed camera and a frame rate of 15.15 kfps can be experimentally verified. Also, the proposed system is applied to monitor the ignition process, and the dynamical responses agree well with that of a photodetector.

II. Methodology

A. Hardware Configuration of the Agile ECT System

As depicted in Fig. 1, the proposed agile ECT hardware system includes N channels of capacitance measurement circuits, a CPCI bus, multiple FPGAs and a host PC. Agile and precise capacitance measurement among different channels and channel switching scheme can be implemented and modified by changing codes in the FPGAs.

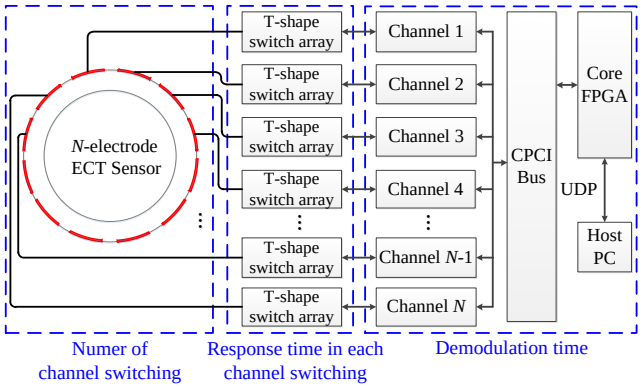

Fig. 1 Schematic of the proposed N-channel parallel agile hardware system for ECT

In each channel, an excitation circuit and a current detection circuit were fabricated and can be detailed in Fig. 2. In the excitation circuit, the sinusoidal voltage excitation signal V_k at fixed frequency f_k in the k-th channel is generated by using a 40 MHz fourteen-bit digital to analog converter (DAC), a low pass filter and a low-noise proportional amplifier. The filter in the excitation circuit is a second-order low-pass filter (LPF), of which the cutoff frequency is 1MHz. Four CMOS switches are controlled by a demodulation FPGA and achieve the signal conditioning in each channel. A T-shape switch array was fabricated to refrain the detected current from the stray capacitances [7, 8], and three switches in the array, i.e. SW_1, SW_2 and SW_3 were coordinated for voltage excitation on the electrode and an individual switch SW_4 shortcuts the measurement signal after the excitation.

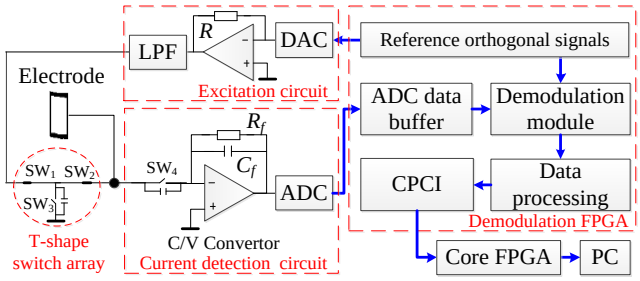

Fig. 2 AC-based capacitance measurement circuit in each channel

The current from the measurement electrode is collected by a current detection circuit. A current to voltage convertor (C/V Convertor) converted the current to a voltage signal. Then, the signal is sampled by utilizing a 40 MHz fourteen-bit analog-to-digital converter (ADC). The sampled data are then stored in the ADC data buffer and bridged to the demodulation module. The amplitudes and phases of the measured signals can be extracted to obtain the mutual capacitances, and the capacitances in each channel are transferred to a core FPGA via a CPCI bus. In the core FPGA, every thousand capacitances are packaged and sent to the host PC via applying the UDP protocol. For all the N channels together, hardware configuration and fast multi-channel measurement can be achieved by implementing the Verilog codes on chip, and the schemes of excitation and demodulations can be varied in the software agilely.

1558-1748 (c) 2018 IEEE. Personal use is permitted, but republication/redistribution requires IEEE permission. See http://www.ieee.org/publications_standards/publications/rights/index.html for more information.

This article has been accepted for publication in a future issue of this journal, but has not been fully edited. Content may change prior to final publication. Citation information: DOI 10.1109/JSEN.2018.2880999, IEEE Sensors Journal

B. Optimal Channel Switching in the Multi-frequency Excitation-measurement Scheme

In the proposed ECT system, each electrode can be set for either excitation or measurement in one cycle of the capacitance measurement, and different excitation and measurement schemes can be applied. In an ECT sensor with N electrodes, there exist $N(N\text{-}1)/2$ independent mutual capacitances, and the number of channel switching should be minimized to shorten the switching time. If the value of N equals to 2^m and m is a positive integer, the least number for the switching to measure all the independent mutual capacitances is m. For the classical single-frequency excitation and measurement scheme, the number of the channel switching is 2^m-1 for 2^m electrodes [13].

The least number of channel switching can be deduced as follows. In one channel switching in an ECT sensor with 2^m electrodes, if k sinusoidal signals are applied on k different excitation electrodes, $k(N\text{-}k)$ mutual capacitances can be measured on the other $N\text{-}k$ measurement electrodes. According to the reciprocity theorem [33], the mutual capacitances remain the same even if the excitation electrodes and the measurement electrodes are exchanged. It means that the number of mutual capacitances can be maximized if k equals to $N\text{-}k$, i.e. $k=N/2=2^{m-1}$. In the same way, the number of mutual capacitances can be maximized for each channel switching, then the number of channel switching can be minimized. Therefore, 2^{m-1} sinusoidal excitation signals at different frequencies applied on 2^{m-1} excitation electrodes is the optimal strategy in the first channel switching. In the first switching, the switches are divided into two groups, each of which has the same number of the electrodes. The mutual capacitances between the two groups were detected, but the mutual capacitance between the electrodes within each group are not measured. So, in the second channel switching, the two groups in the first switching are divided again into four subgroups. Each subgroup has the same number of the electrodes, namely 2^{m-2} electrodes. In the same way as that of the first switching, the mutual capacitances between electrodes in the two subgroups from any one group in the first switching can be detected. Similarly, the same operation can be continued until all the subgroups contains only one electrode, then all mutual capacitances are measured. Since each group can be divided into two subgroups in every channel switching, for all the 2^m electrodes, m times are needed to divide all the 2^m electrodes into individual electrodes. In general, for an ECT sensor with N electrodes, the least number of channel switching can be expressed as

$$N_s = m, \left(2^{m-1} \le N \le 2^m\right), \tag{1}$$

and the deduction process is quite like that of the fast Fourier transform. As a result, the measurement time of all mutual capacitances using the proposed strategy is $m/(2^m\text{-}1)$ of the time via using the classical scheme.

Take the ECT sensor with sixteen electrodes as an example, the least number of channel switching is four. The electrodes are indexed clock-wisely and subscripted from 1 to 16. The process for all the four switching is detailed in Fig. 3. In the first switching, the electrodes indexed by E_1, E_2, E_5, E_6, E_9, E_{10}, E_{13} and E_{14} are selected as the excitation group, while the other eight electrodes are used for capacitance measurements. Then in the second switching, the excitation group is divided into two equal subgroups, and electrodes indexed by E_1, E_5, E_9 and E_{13} are used as the measurement subgroup. In the third switching, electrodes E_1 and E_5 are used for excitation again, and the mutual capacitance between them is measured in the four switching. As a result, all the mutual capacitances can be achieved through four switching. Compared with the signal-frequency parallel ECT system with sixteen electrodes, the switching number can be reduced from fifteen to four, and it helps to improve the frame rate.

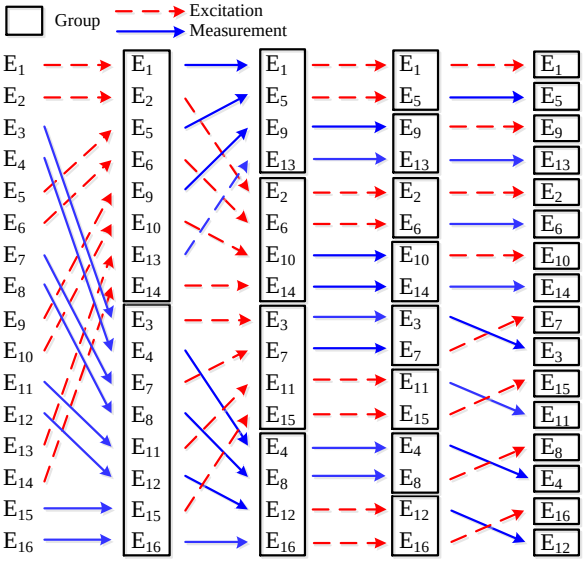

Fig. 3 Optimal channel switching in the multi-frequency excitation and measurement scheme in the sixteen-electrode ECT system

C. Response Time in each Channel Switching

A grounding strategy was proposed to shorten the response time in each channel switching of the classical consequent excitation. After each capacitance measurement, the input of the current detectors was grounded for a short-time discharging, and then switched for the next capacitance measurement. The sampling operations waited until the signal of the current detector was stabilized for the charging. The response time of each switching consisted of both the discharging and the charging time. In a single channel for capacitance measurement, a small standard deviation, i.e. 0.11 fF can be achieved for a 200fF ceramic capacitor excited at 100 kHz. For multi-channels in the ECT system, the channel switching tended to amplify the deviations, and they declined for an increased response time of the electronic switches, see the curves plotted in Fig. 4. The grounding scheme proposed here accelerated the dropping of the deviations as the switching time was prolonged. The deviations also decreased for a rising value of the discharging time, even if the discharging was partially implemented for only 50 ns, a better performance over the ungrounded case was achieved. However, when the discharging was prolonged from 125 ns to 2.5 μs, the deviations started to be stable and only saw a slight decrease. If the grounding strategy was not applied, the response time should be over 15 μs to suppress the standard

1558-1748 (c) 2018 IEEE. Personal use is permitted, but republication/redistribution requires IEEE permission. See http://www.ieee.org/publications_standards/publications/rights/index.html for more information.

This article has been accepted for publication in a future issue of this journal, but has not been fully edited. Content may change prior to final publication. Citation information: DOI 10.1109/JSEN.2018.2880999, IEEE Sensors Journal

deviations within 0.13fF. In the proposed ECT system, the discharging time is set as 125 ns and the response time is set as 7.5μs, to achieve a similar standard deviation, i.e. 0.13fF as the single channel.

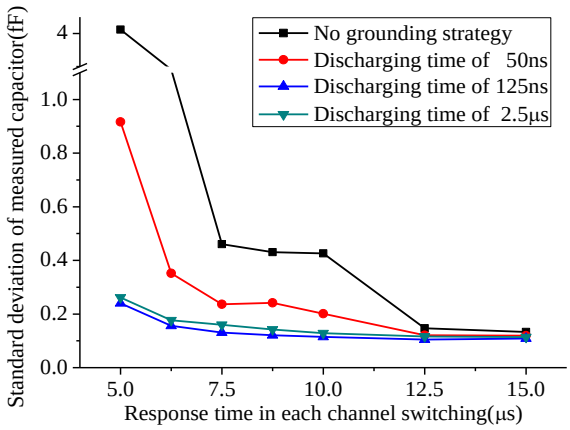

Fig. 4 Standard deviations in measuring a 200fF ceramic capacitor for different discharging time and the response time in channel switching

III. System Performance Evaluation

In this work, the frequencies used for the excitation were optimized and selected for image reconstruction, and the agile hardware was fabricated to implement all the schemes mentioned above, and the functions of the hardware can be updated by running specifically designed Verilog codes.

A. An agile Excitation-measurement Card for precise capacitance measurement

To implement multi-frequency excitation-measurement strategies in hardware, an agile excitation-measurement card was designed, as shown in Fig. 5. In the card, the measurement board and an excitation board were connected through pin connectors. The measurement board consisted of four independent capacitance detection circuits, a demodulation FPGA and a CPCI interface. On the excitation board, four excitation circuits in the excitation board generated sinusoidal voltage excitation signals. Each current detection circuit utilizing a 14-bit ADC was uniquely connected to an excitation circuit for one channel. The signal-to-noise ratio (SNR) was used here to compare the desired signal with background noise, and it was defined as

$$\mathrm{SNR} = 10\log\frac{\sum_{m=1}^{M} C(m)^2}{\sum_{m=1}^{M}\left[C(m)-\frac{1}{M}\sum_{m=1}^{M}C(m)\right]^2} \qquad (2)$$

where $C(m)$ is the m-th measured capacitance, M is the total number of repetitive measurements [34]. From the definition, it implies that the SNR increases if values of the capacitance is increasing for the same noise level.

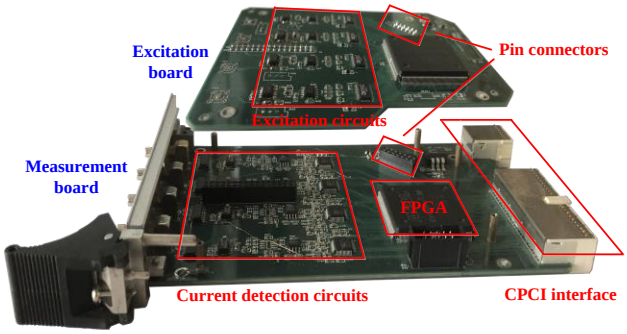

Fig. 5 Photo of the proposed agile excitation-measurement card

The resolution of measured capacitances depends not only on the effective number of bits in the ADC but also the number of samples used in the modulations. One hundred repetitive voltage data contaminated with a 10mV Gaussian noise were generated to evaluate the performance of different number of ADC bits, as shown in Fig. 6. Four different capacitances, i.e. 50fF, 300fF, 1000fF and 3000fF were used, and in all the four cases, the value of measurement SNR stabilized if the number of ADC bits was over eight. As a result, the effective number of bits in the selected ADC can be ignored on the resolution of the measured capacitances, and the 14-bit ADCs used here were sufficient for precise capacitance measurement.

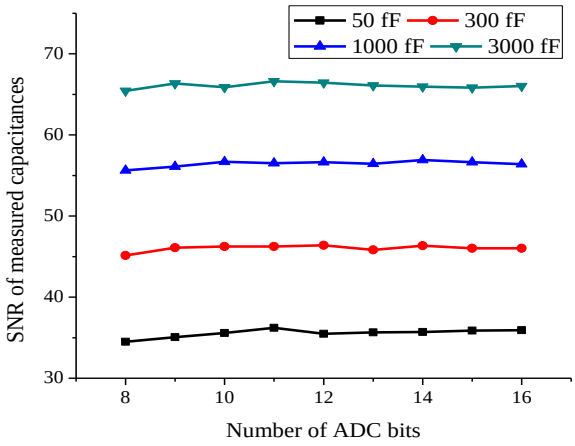

Fig. 6 SNR of measured capacitances for different number of ADC bits in cases of four capacitances.

Nine ceramic capacitors ranging from about 0.07pF to 3pF were calibrated by the impedance analyzer Agilent 4294A, and were used to evaluate the linearity of the circuits. After calibrated at every used frequency, the measured capacitances can be in the same precision. For example, if the electrode in channel 1 was excited at the frequency of 100 kHz, the values of the capacitances were plotted against their measurement in Fig. 7 and the data were listed in Table 1. In the linear regression, the correlation coefficient between the actual values and the measured data was 0.99999987, the SNR climbed from 40 dB to 77 dB and the standard deviation fluctuations between 0.15 fF and 0.18 fF as the measured capacitances were increased from 0.07 pF to 3.3 pF. The results verified that the proposed agile card could achieve the same accuracy as that of the single-frequency measurement in typical AC-based single-frequency ECT systems [13].

1558-1748 (c) 2018 IEEE. Personal use is permitted, but republication/redistribution requires IEEE permission. See http://www.ieee.org/publications_standards/publications/rights/index.html for more information.

This article has been accepted for publication in a future issue of this journal, but has not been fully edited. Content may change prior to final publication. Citation information: DOI 10.1109/JSEN.2018.2880999, IEEE Sensors Journal

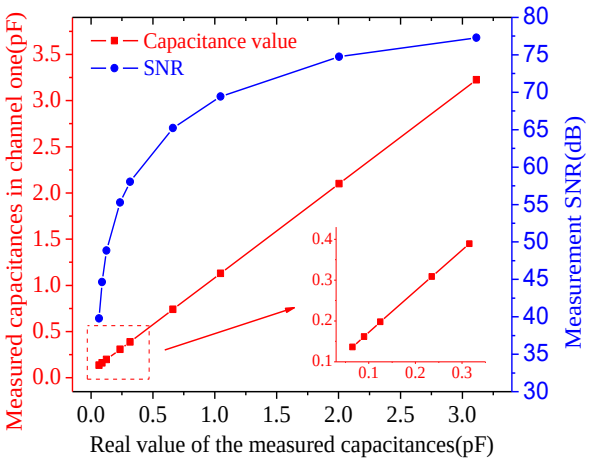

Fig. 7 Values of measured capacitances and its SNR for nine ceramic capacitors

Table 1 Measured value and SNR for nine actual capacitances

Actual capacitances (fF)	Measured values (fF)	SNR (dB)	Actual capacitances (fF)	Measured values (fF)	SNR (dB)
65.9	66.3	39.8	662.2	670.4	65.2
92.3	91.7	44.6	1046.8	1059.5	69.4
125.0	127.8	48.9	2005.0	2030.6	74.8
235.1	238.7	55.3	3113.9	3153.8	77.3
315.5	319.1	58.0			

Although each channel was fabricated in the same way, parameter fluctuations still existed among the measurement circuits in different channels. Measurement circuit in each channel was calibrated respectively, at all the used frequencies ranging from 100 kHz to 600 kHz, and the standard deviations of the calibrated capacitors were listed in Table 2. It showed that the deviated values at all frequencies were within 0.2 fF and those at 200 kHz and 300 kHz were slightly smaller. It might lie in the fact that these two frequencies were in the middle of the passband of the current to voltage converter, which was set to be suitable for the middle frequency signals to achieve better overall performance.

Table 2 Standard deviation of the measured capacitances at six different excitation frequencies

Measured capacitance (fF)	Standard deviation at different excitation frequencies(kHz)					
	100	200	300	400	500	600
40.20	0.14	0.08	0.11	0.14	0.13	0.15
65.60	0.16	0.10	0.10	0.13	0.12	0.15
104.20	0.17	0.10	0.10	0.13	0.11	0.15
212.20	0.16	0.10	0.09	0.13	0.12	0.16
287.30	0.17	0.09	0.09	0.14	0.14	0.13
630.00	0.17	0.09	0.09	0.14	0.12	0.14
1019.10	0.16	0.09	0.09	0.14	0.17	0.17
1977.50	0.16	0.10	0.11	0.15	0.22	0.14
3088.40	0.15	0.11	0.11	0.19	0.13	0.15

B. Multi-frequency excitation in the proposed Agile Parallel ECT System

In typical ECT systems, the frequencies of the excitation signals usually range from several kHz to 1 MHz [36]. Due to the bandwidth limitation of the C/V converter, the highest excitation frequency here was set to be 600kHz. The lowest frequency for the multiple frequency excitation is optimized to minimize the condition number of the inverse state-error correlation matrix in the non-integer-period demodulation [31, 32]. For a twelve-electrode sensor, six different frequencies are applied on the excitation electrodes at the same time, the frequencies are equally spaced. The condition number bottomed at 100kHz in this case, see the black line in Fig. 8, and the frequencies of the excitation signal are selected from 100 kHz to 600 kHz with a step of 100 kHz. Eight different frequencies were applied to the sixteen-electrode ECT system, to minimize the condition number, if the frequencies were equally spaced between 75 kHz and 600 kHz. Generally, the condition number reaches its minimum, if the lowest frequency is set as $2f_{max}/N$, where f_{max} and N are respectively the highest excitation frequency and the number of electrodes.

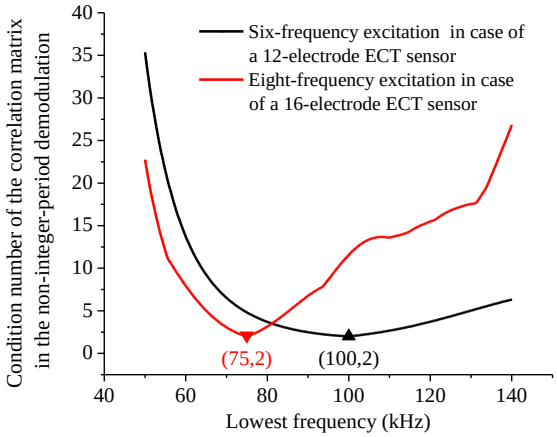

Fig.8 Condition number of the correlation matrix in the non-integer-period demodulation for a varying lowest frequency

To fabricate a sixteen-electrode ECT system, four agile excitation-measurement cards were synchronized through the CPCI interface. Then, a unique excitation channel and a unique measurement channel can be connected to each electrode in the sensor, and a multi-frequency ECT system for less than sixteen electrodes can be configured via using the Verilog codes in the FPGA, see Fig. 9. For ECT sensors of twelve and sixteen electrodes used in this work, the angular widths of the electrodes were respectively 0.48 and 0.37, and the diameter and the length of the electrodes were both 100 mm. For a twelve-electrode ECT sensor, the standing capacitance values, capacitance values measured by the proposed ECT system and SNR of the measured capacitance values between electrodes were listed in Table 3. The SNR varied from 30.5 dB to 66.8 dB for an increasing value of mutual capacitance from 11.4fF to 2726 fF, which dynamically ranged for the ECT measurement.

1558-1748 (c) 2018 IEEE. Personal use is permitted, but republication/redistribution requires IEEE permission. See http://www.ieee.org/publications_standards/publications/rights/index.html for more information.

This article has been accepted for publication in a future issue of this journal, but has not been fully edited. Content may change prior to final publication. Citation information: DOI 10.1109/JSEN.2018.2880999, IEEE Sensors Journal

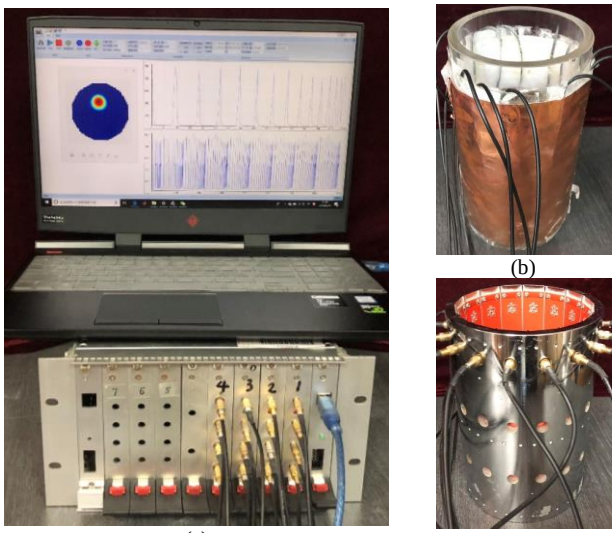

(a) (b) (c)

Fig. 9 Overall ECT system used for experiments. (a) The host computer and ECT system (b) The 12-electrode ECT sensor (c) The 16-electrode ECT sensor

Table 3. Standing capacitances, measured capacitances and SNR of measured capacitances for the 12-electrode ECT sensor. The unit for all the capacitances in the table is fF. C_s and C_m are respectively standing capacitance values of the 12-electrode ECT sensor and the measured capacitances from the proposed system.

C_s	C_m	SNR	C_s	C_m	SNR	C_s	C_m	SNR
2727	2726	66.8	81.7	80.6	40.3	28.4	27.3	34.2
15.9	14.8	32.9	13.1	12.0	30.8	11.8	10.7	30.6
12.3	11.2	30.9	16.9	15.8	32.0	32.8	31.7	34.0
89.5	88.4	39.3	2530	2529	65.8	2416	2415	66.8
82.9	81.8	39.3	26.9	25.8	34.6	17.3	16.2	32.0
12.9	11.8	31.0	11.7	10.6	31.0	13.4	12.3	30.9
21.6	20.5	32.3	34.6	33.5	33.7	83.0	81.9	39.2
2733	2732	66.5	79.1	78.0	39.7	29.0	27.9	33.9
16.6	15.5	32.1	12.6	11.5	30.9	12.5	11.4	30.5
17.5	16.4	31.1	22.5	21.4	31.7	28.1	27.0	33.8
2747	2746	65.6	88.3	87.2	39.6	28.6	27.5	33.7
17.4	16.3	31.8	13.8	12.7	31.0	16.6	15.5	30.8
18.5	17.4	31.2	17.1	16.0	31.7	2372	2371	66.4
75.2	74.1	39.5	26.5	25.4	33.5	16.7	15.6	31.8
17.1	16.0	30.8	16.9	15.8	30.9	12.6	11.5	31.1
2561	2560	67.2	80.9	79.8	39.6	28.9	27.8	33.6
22.1	21.0	31.4	18.6	17.5	30.7	12.1	11.0	30.7
2014	2013	66.2	78.5	77.4	39.1	32.9	31.8	33.6
22.3	21.2	31.7	12.5	11.4	30.9	2259	2258	65.9
87.3	86.2	39.8	34.4	33.3	34.1	16.4	15.3	31.6
2451	2450	65.5	89.0	87.9	38.7	27.4	26.3	33.5
2746	2745	66.0	82.1	81.0	39.0	2744	2743	65.2

An acrylic rod with a diameter of two centimeters was located at three different positions, to evaluate the image reconstructions from the mutual capacitances in ECT sensors. The Landweber algorithm was implemented to reconstruct the images of its cross-sectional profile, in cases of both 12 and 16 electrodes[35]. In the reconstructed images, as illustrated in Fig. 10, gray values with maximum latitude were drawn with black circles reflecting the position and size of the rod. The reconstructed profiles of the rod at different locations can be correctly identified from the measured capacitances by using the proposed system.

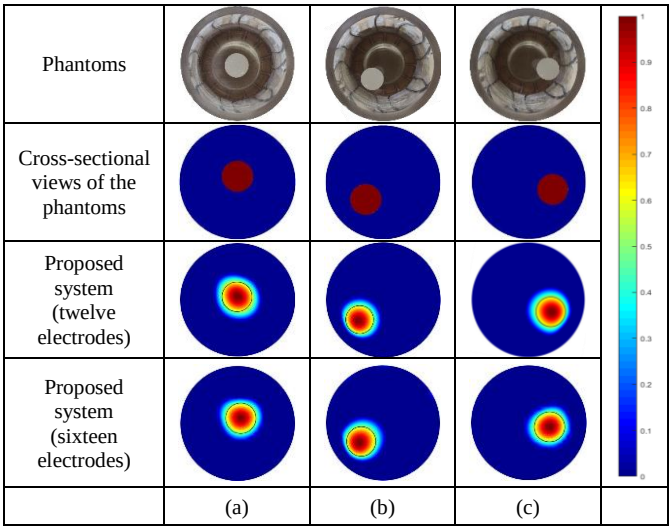

Fig. 10 Images of the rod reconstructed by both twelve and sixteen electrodes in the proposed system.

C. Frame Rate and Experimental Verification

For a single-frequency multi-channel parallel ECT system, the frame rate v_s can be calculated by

$$v_s = \frac{1}{(T_r + T_{demo}) \cdot (N-1)} . \quad (3)$$

where T_r and T_{demo} are respectively the response time of electronic switches and demodulation time in each channel switching. The frame rate can be improved for a multi-frequency multi-channel parallel ECT system, and derived as

$$v_m = \frac{1}{(T_g + T_{demo-non}) \cdot N_s} , \quad (4)$$

where T_g is the response time for the grounding strategy and set as 7.5μs. N_s is the least number of channel switching calculated from (1), $T_{demo\text{-}non}$ is the demodulation time in the case that 0.9 periods of sampled points are used for non-integer-period demodulation. If the excitation frequencies are stepped at 600/(N/2) kHz from 600/(N/2) kHz to 600 kHz, then the values of $T_{demo\text{-}non}$ can be derived from

$$T_{demo-non} = \frac{0.9}{6\times10^5/(N/2)} \times 10^6 = \frac{3N}{4} \ \mu s \quad (5)$$

The lowest frequencies in the cases of twelve and sixteen electrodes were 100 kHz and 75 kHz respectively, and the values of $T_{demo\text{-}non}$ were 9μs and 12μs. As a result, the frame rate for the twelve electrodes reached 15.15k fps, it dropped to be 12.82k fps if the electrode number increased to be sixteen.

Fig. 11 showed that the frame rate decreases for an increasing electrode number for both the traditional multi-channel ECT system and the proposed agile system. Once the electrode number is fixed, the multi-frequency multi-channel parallel ECT system is about twice faster at the same precision, due to the proposed optimal channel switching scheme, grounded switching strategy and the non-integer-

1558-1748 (c) 2018 IEEE. Personal use is permitted, but republication/redistribution requires IEEE permission. See http://www.ieee.org/publications_standards/publications/rights/index.html for more information.

This article has been accepted for publication in a future issue of this journal, but has not been fully edited. Content may change prior to final publication. Citation information: DOI 10.1109/JSEN.2018.2880999, IEEE Sensors Journal

period demodulation. If less sampled points are used for the demodulation, the demodulation time $T_{demo\text{-}non}$ can be shortened and the frame rate can be improved at an expanse of larger standard deviations.

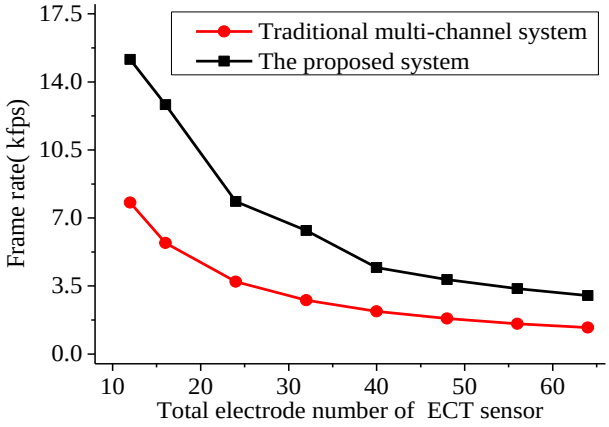

Fig. 11 Frame rate of ECT systems versus electrode number in the sensor with respect to the demodulation time and the response time of switches

Frame rates of ECT systems published in the literature were compared with the proposed agile system and listed in Table 4. In the traditional cascade and parallel ECT systems, only one excitation channel, the single-electrode multi-frequency excitation strategy can be implemented in hardware. However, the multi-electrode excitation strategy cannot be implemented before the grounding strategy was proposed in this work. Moreover, for a *N*-electrode ECT sensor, the proposed agile parallel ECT system enabled independent excitation and measurement in each individual channel, not only the strategy implemented in the traditional ECT system can be achieved, but also more flexible multi-electrode multi-frequency excitation strategy can be implemented.

Table 4 Frame rate of ECT systems proposed in literatures and this work

Year	System mode	Electrodes	Frame rate(fps)	N_e*	N_m*	Reference
2012	Cascade	12	185	1	1	Zhou *et al* [7]
2009	Parallel	12	1400	1	12	Wang *et al* [37]
		16	2200	1	16	
2011		16	1542	1	16	Cui *et al* [24]
2017		16	1250	1	16	Kryszyn *et al* [12]
		12	11000	1	12	Sun *et al* [13]
This work	Agile parallel	12	15150	12	12	-
		16	12820	16	16	-

* N_e is the number of voltage excitation channels
N_m is the number of current measurement channels

To verify the frame rate proposed in this work, a glowing golf ball falling process was measured by the 15150 fps high-speed camera and the proposed ECT system at the same time, and the projections of the cross-sectional images of both ECT and camera are used for comparison. In the experiment, a LED lamp was installed in a golf to strengthen the image quality of the high-speed camera. When the glowing ball falls, as shown in Fig. 12, the high-speed camera captured projected images of the ball at a speed of 15150 frames per second. A slit of 103mm×3.5mm in a traditional ECT sensor was conserved for the high-speed camera, as shown in Fig.13.

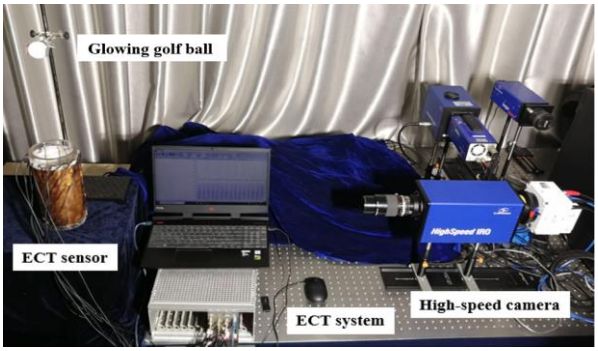

Fig. 12 Experimental setup used for comparisons of the ECT system and a high-speed camera in a glowing golf ball free falling

The ball fell above the sensor, and the high-speed camera and the proposed 12-electrode ECT system were operated at the same time. The image reconstructed by ECT can be regarded as on the cross section at the center of the region of interest, but only the gray values projected on the x-axis are used for comparison, as depicted in Fig. 13(a). The images reconstructed by the proposed ECT system and taken by the high-speed camera are compared in Fig. 14. The variation measured by the ECT system agrees well with that obtained by the high-speed camera. In Fig. 15, normalized gray values projected on the x-axis were depicted for the images of both ECT system and high-speed camera in the process of the ball free falling and rebounding. No delay time appeared between them and the peaks of the two curves agree well with each other at the same time.

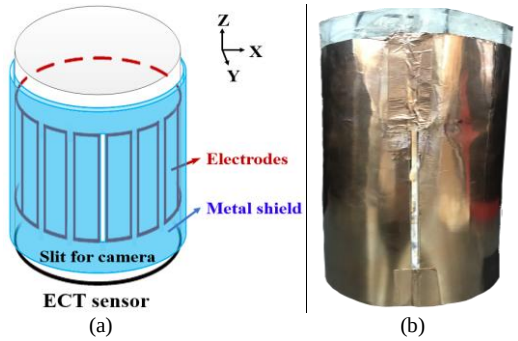

(a) (b)

Fig. 13 Twelve-electrode ECT sensor with a 103mm×3.5mm slit fabricated on the metal shield used for the experiment. (a) Detailed structure of the ECT sensor (b) Photo of the ECT sensor

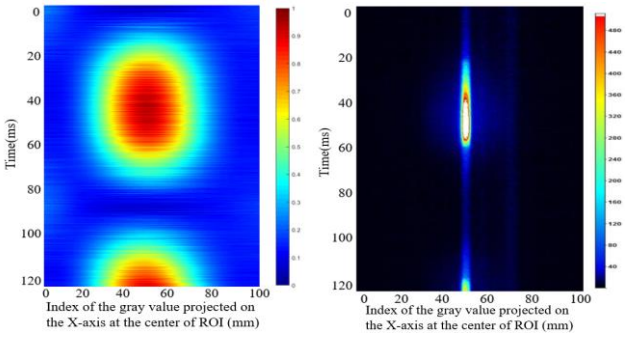

(a) (b)

Fig. 14 Projected images of the free dropping ball along the x-axis of both proposed ECT system and the high-speed camera. (a) the proposed ECT system and (b) the high-speed camera

1558-1748 (c) 2018 IEEE. Personal use is permitted, but republication/redistribution requires IEEE permission. See http://www.ieee.org/publications_standards/publications/rights/index.html for more information.

This article has been accepted for publication in a future issue of this journal, but has not been fully edited. Content may change prior to final publication. Citation information: DOI 10.1109/JSEN.2018.2880999, IEEE Sensors Journal

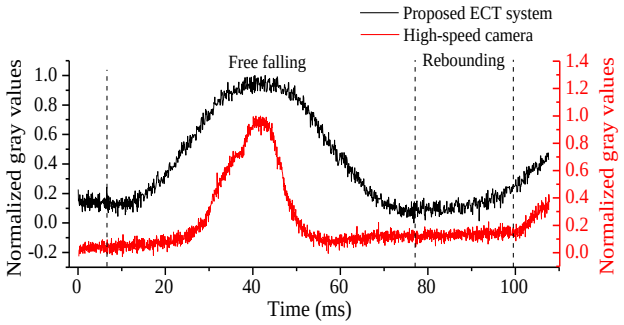

Fig. 15 Normalized gray values projected on the x-axis for the images of both ECT system and high-speed camera in the process of the ball free falling and rebounding. These two curves were deliberately separated a bit for better visual comparisons.

D. Flame Ignition Monitoring via using the Proposed System

The experimental setup to monitor the dynamical process of the ignited flame was illustrated in Fig. 16. The proposed high speed agile ECT system monitored the ignition process of the flame in a Bunsen burner, at a frame rate of 15.15k fps, and details of the ignition process were captured.

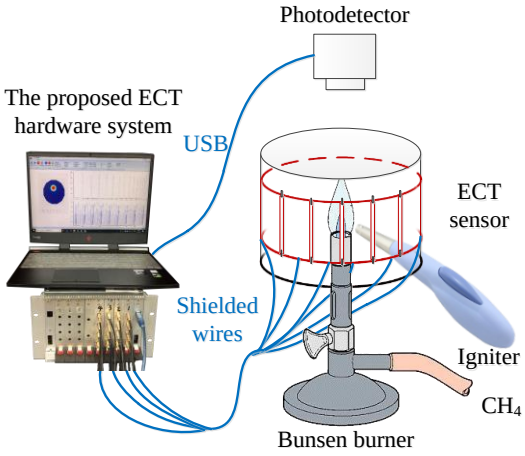

Fig. 16 Experimental setup for ignition process monitoring

To compare the reconstructed results of the proposed system and the traditional parallel system, the temporal variations in averaged relative permittivity in the ignition process measured by the two systems were compared in Fig. 17(a). The pulses of high relative permittivity can be seen clearly by the variation measured by the proposed system. The interval of two neighboring pulses is about 30 micro-seconds. Usually, the averaged relative permittivity pulse was undistinguishable in a low-speed ECT system. The temporal variations of the reconstructed relative permittivity distributions were depicted in three dimensions, as shown in Fig. 17(b). The two-dimensional images were interpolated along the time. It implied that the flame was generated after each ignition and then expanded for about 100ms and the expanded flame stabilized after 330 ms. The proposed ECT system is capable to obtain more details than the low speed system.

To find out the source of the high relative permittivity pulse, a dynamic experiment with only ignitions was carried out. The electronic pulse igniter ignited in the ECT sensor. A photodetector was used along with the ECT system to

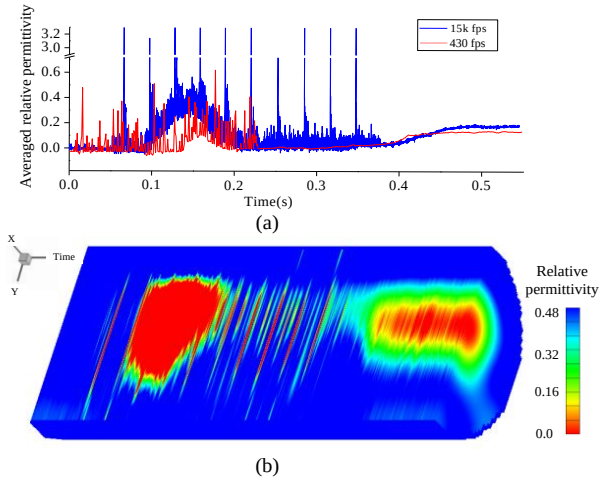

Fig. 17 Measured data of the ignition flame via using the proposed system and the low-speed system. (a) The temporal variations in averaged relative permittivity and (b) the temporal variations of the reconstructed relative permittivity distributions

simultaneously monitor the ignition pulses. The proposed system reconstructed the images of relative permittivity and the photodetector captured the light generated by the igniter, and the results were compared in Fig. 18.

As was depicted in Fig. 18(a), the variations measured by the system agreed well with that obtained by the photodetector. It indicated that the pulses in the signals were raised by the electronic pulse igniter. The igniting interval was about 30ms and the temporal variations of the reconstructed relative permittivity distributions were three dimensionally illustrated in Fig. 18(b).

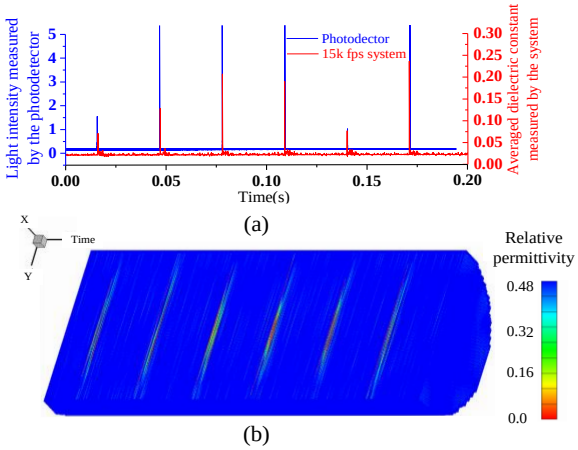

Fig. 18 Measured data of the ignition signals via using the proposed system and the photodetector. (a) The variations measured by the system and the photodetector and (b) the temporal variations of the reconstructed relative permittivity distribution achieved by the proposed system.

IV. Conclusion

In this paper, an agile multi-frequency and multi-channel parallel ECT system was proposed, and it can have a high capacitance acquisition rate of up to 15.15k fps. The number of channel switching is minimized to speed up the multichannel capacitance acquisitions. The grounding strategy was applied to discharge useless electrical charges and the response time of the channel switching can be reduced. When sampled data in 0.9 periods is used for demodulation, the imaging rate of the

1558-1748 (c) 2018 IEEE. Personal use is permitted, but republication/redistribution requires IEEE permission. See http://www.ieee.org/publications_standards/publications/rights/index.html for more information.

This article has been accepted for publication in a future issue of this journal, but has not been fully edited. Content may change prior to final publication. Citation information: DOI 10.1109/JSEN.2018.2880999, IEEE Sensors Journal

twelve- and sixteen-electrode system reaches 15.15 kfps and 12.82 kfps, respectively. Different number of electrodes can be flexibly adjusted and manipulated by the FPGA in the system. The proposed ECT system was used to monitor the ignition process of a flame generated by a Bunsen burner. Discharge processes of the igniter have been captured and the results of the ignition pulses agreed well with those of the photodetector. The proposed hardware system provides an agile way to integrate the channel switching, the demodulation and the sensor configuration on a single chip, i.e. an FPGA. The major limitation of the proposed technique is that the system might fail to work when the measured object is frequency-sensitive. However, for flame, fluidized beds, good images with high temporal resolution can be obtained by the proposed ECT system. Also, the proposed ECT system can be further applied to 3D imaging to improve the frame rate.

REFERENCES

[1] I. Saied and M. Meribout, "Electronic hardware design of electrical capacitance tomography systems," Philosophical Transactions, 374, p. 20150331, (2016).

[2] M. V. Sardeshpande, S. Harinarayan and V. V. Ranade, "Void fraction measurement using electrical capacitance tomography and high speed photography," Chemical Engineering Research & Design, 94, pp. 1-11, (2015).

[3] D. Xie, Z. Huang, H. Ji, and H. Li, "An Online Flow Pattern Identification System for Gas–Oil Two-Phase Flow Using Electrical Capacitance Tomography," IEEE Transactions on Instrumentation & Measurement, 55, pp. 1833-1838, (2006).

[4] M. Meribout and I. M. Saied, "Real-time Two Dimensional Imaging of Solid Contaminants in Gas Pipelines using An Electrical Capacitance Tomography System," IEEE Transactions on Industrial Electronics, PP, p. 1-1, (2017).

[5] M. Mao, J. Ye, H. Wang, and W. Yang, "Investigation of gas–solids flow in a circulating fluidized bed using 3D electrical capacitance tomography," Measurement Science & Technology, 27, p. 095401, (2016).

[6] S. Liu, Q. Chen, X. Xiong, Z. Zhang, and J. Lei, "Preliminary study on ECT imaging of flames in porous media," Measurement Science & Technology, 19, p. 094017, (2008).

[7] H. Zhou, L. Xu, Z. Cao, X. L. Liu, and S. Liu, "A complex programmable logic device-based high-precision electrical capacitance tomography system," Measurement Science & Technology, 24, p. 074006, (2013).

[8] W. Q. Yang, "Hardware design of electrical capacitance tomography systems," Measurement Science & Technology, 7, p. 225, (1999).

[9] X. Yue and C. Mcleod, "FPGA design and implementation for EIT data acquisition," Physiological Measurement, 29, p. 1233, (2008).

[10] M. Meribout and S. Teniou, "A Pipelined Parallel Hardware Architecture for 2-D Real-Time Electrical Capacitance Tomography Imaging Using Interframe Correlation," IEEE Transactions on Very Large Scale Integration Systems, 25, pp. 1320-1328, (2017).

[11] J. Kryszyn, D. Wanta and W. T. Smolik, "Gain Adjustment for Signal-to-Noise Ratio Improvement in Electrical Capacitance Tomography System EVT4," IEEE Sensors Journal, vol. 17, p. 8107 - 8116, (2017).

[12] J. Kryszyn, P. Wróblewski, M. Stosio, D. Wanta, T. Olszewski, and W. T. Smolik, "Architecture of EVT4 data acquisition system for electrical capacitance tomography," Measurement, 101, pp. 28-39, (2017).

[13] S. Sun, Z. Cao, A. Huang, L. Xu, and W. Yang, "A High-speed Digital Electrical Capacitance Tomography System Combining Digital Recursive Demodulation and Parallel Capacitance Measurement," IEEE Sensors Journal, vol. 17, p. 6690–6698, 2017.

[14] A. Mcewan, J. Tapson, S. A. Van, and D. S. Holder, "Code-division-multiplexed electrical impedance tomography spectroscopy.," IEEE Transactions on Biomedical Circuits & Systems, 3, p. 332, (2009).

[15] M. S. Tsoeu and M. R. Inggs, "Fully Parallel Electrical Impedance Tomography Using Code Division Multiplexing," IEEE Trans Biomed Circuits Syst, 10, p. 556, (2016).

[16] H. Wang, S. Xin and X. Zhang, "New progress of the digital electrical capacitance tomography system for gas/liquid two phase flow," in *IEEE International Workshop on Imaging Systems and Techniques*, 2009, pp. 37-40.

[17] R. Rasel, C. Zuccarelli, Q. Marashdeh, L. S. Fan, and F. Teixeira, "Towards Multiphase Flow Decomposition Based on Electrical Capacitance Tomography Sensors," IEEE Sensors Journal, vol. 17, p. 8027–8036, 2017.

[18] R. K. Rasel, C. Gunes, Q. M. Marashdeh, and F. L. Teixeira, "Exploiting the Maxwell-Wagner-Sillars Effect for Displacement-Current Phase Tomography of Two-Phase Flows," IEEE Sensors Journal, vol. 17, p. 7317 - 7324, (2017).

[19] M. Zhang and M. Soleimani, "Simultaneous reconstruction of permittivity and conductivity using multi-frequency admittance measurement in electrical capacitance tomography," Measurement Science & Technology, 27, p. 025405, (2016).

[20] B. Han, Y. Xu and F. Dong, "Design of current source for multi-frequency simultaneous electrical impedance tomography.," Review of Scientific Instruments, 88, p. 094709, (2017).

[21] Z. Fan and R. X. Gao, "Enhancement of Measurement Efficiency for Electrical Capacitance Tomography," IEEE Transactions on Instrumentation & Measurement, 60, pp. 1699-1708, (2011).

[22] J. Jia and M. Wang, "An optimisation method for the over-zero switching scheme," Flow Measurement & Instrumentation, 27, pp. 47-52, (2012).

[23] M. Wang and Y. Ma, "Over-zero switching scheme for fast data collection operation in electrical impedance tomography," Measurement Science & Technology, 17, p. 2078, (2006).

[24] Z. Cui, H. Wang, Z. Chen, Y. Xu, and W. Yang, "A high-performance digital system for electrical capacitance tomography," Measurement Science & Technology, 22, p. 055503, (2011).

[25] R. Halter, A. Hartov and K. D. Paulsen, "Design and implementation of a high frequency electrical impedance tomography system.," Physiological Measurement, 25, pp. 379-390, (2004).

[26] Y. Yang, F. Zhang, K. Tao, L. Wang, H. Wen, and Z. Teng, "Multi-frequency simultaneous measurement of bioimpedance spectroscopy based on a low crest factor multisine excitation.," Physiological Measurement, 36, p. 489, (2015).

[27] B. Sanchez, G. Vandersteen, R. Bragos, and J. Schoukens, "Basics of broadband impedance spectroscopy measurements using periodic excitations," Measurement Science & Technology, 23, pp. 105501-105514(14), (2012).

[28] S. Khan, P. Manwaring, A. Borsic, and R. Halter, "FPGA-based voltage and current dual drive system for high frame rate electrical impedance tomography," IEEE Trans Med Imaging, 34, pp. 888-901, (2015).

[29] L. Xu, H. Zhou, Z. Cao, and W. Yang, "A Digital Switching Demodulator for Electrical Capacitance Tomography," IEEE Transactions on Instrumentation & Measurement, 62, pp. 1025-1033, (2013).

[30] D. Zheng, S. Zhang, S. Wang, C. Hu, and X. Zhao, "A Capacitive Rotary Encoder Based on Quadrature Modulation and Demodulation," IEEE Transactions on Instrumentation & Measurement, 64, pp. 143-153, (2014).

[31] L. Xu, H. Zhou and Z. Cao, "A recursive least squares-based demodulator for electrical tomography.," Review of Scientific Instruments, 84, p. 418, (2013).

[32] S. Sun, L. Xu, Z. Cao, A. Huang, and W. Yang, "Digital Recursive Demodulator Based on Kalman Filter," IEEE Transactions on Instrumentation & Measurement, vol. 66, p. 3138 - 3147, (2017).

[33] D. B. Geselowitz, "An application of electrocardiographic lead theory to impedance plethysmography," IEEE transactions on bio-medical engineering, 18, pp. 38-41, (1971).

[34] A. Yusuf, D. Sudiana, A. S. Tamsir, and S. H. Sudibyo, "Analysis of excitation frequency to performance of electrical capacitance tomography," in *International Conference on Information Technology and Electrical Engineering*, 2017, pp. 1-4.

[35] H. Zhou, L. Xu, Z. Cao, X. L. Liu, and S. Liu, "A complex programmable logic device-based high-precision electrical capacitance tomography system," Measurement Science & Technology, 24, p. 074006, (2013).

[36] W. Q. Yang and L. Peng, "Image reconstruction algorithms for electrical capacitance tomography," Measurement Science & Technology, 14, pp. 478-484, (2004).

[37] B. Wang, Z. Huang and H. Li, "Design of high-speed ECT and ERT system,", Journal of Physics: Conference Series, 2009, p. 012035.

1558-1748 (c) 2018 IEEE. Personal use is permitted, but republication/redistribution requires IEEE permission. See http://www.ieee.org/publications_standards/publications/rights/index.html for more information.

This article has been accepted for publication in a future issue of this journal, but has not been fully edited. Content may change prior to final publication. Citation information: DOI 10.1109/JSEN.2018.2880999, IEEE Sensors Journal

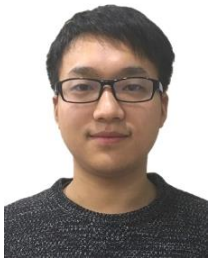

Ang Huang received the B.Sc. degree in Instrument Science and Opto-Electronic Engineering and Honor College, Beihang University, Beijing, China, in 2016. Currently, he is working there toward the Ph.D. degree. His research interests include hardware design of high performance electrical and optical tomography systems.

Zhang Cao (M'10–) received the B.Sc. degree (with distinction) in automation and the M.Eng. and Ph.D. degrees (with distinctions) in measurement technology and automatic devices from Tianjin University, Tianjin, China, in 2003, 2005, and 2008, respectively. From 2008, he works for Beihang University, Beijing, China. At present, he is a professor with the School of Instrumentation Science and Opto-Electronic Engineering, Beihang University.

His research interests include process tomography, multiphase flow measurement, and inverse problems.

Shijie Sun (M'17–) received the B.Sc. degree in automation from Tianjin University, Tianjin, China, in 2011 and received the Ph.D. degree in measurement technology and instruments from Beihang University, Beijing, China, in 2017. He is currently a post-doctor in Beihang University, Beijing, China.

His current research interests include electrical tomography and digital signal processing.

Fanghao Lu received the B.Sc. degree in Instrument Science and Opto-Electronic Engineering Beihang University, Beijing, China, in 2017. Currently, he is a postgraduate in Beihang University. His research interests include the digital signal processing and the hardware design of the electrical and optical detection systems.

Lijun Xu (M'04–SM'04) received the BSc, MEng, and PhD degrees in electrical engineering and instrumentation from Tianjin University, Tianjin, China, in 1990, 1993 and 1996, respectively.

From 1997 to 2001, he was an associate professor with Tianjin University. From Jan 2002 to Apr 2006, he was a research fellow with University of Greenwich, University of Kent, and a higher scientific officer with Institute of Cancer Research, UK. He is currently a professor and the Dean of the School of Instrumentation Science and Opto-Electronic Engineering, Beihang University, Beijing, China. He has authored or coauthored more than 260 publications. His current research interests include tomographic imaging, scanning imaging and dynamic process monitoring.

Dr. Xu won the National Science Fund for Distinguished Young Scholars, the Ministry of Education Technology Invention Award (1st class) and China Instrument Society Science and Technology Award (1st class) in 2012, 2012 and 2014, respectively. He was elected as a Chang-Jiang Scholars Program Professor and a National High-Level Personnel of Special Support Program by the Ministry of Education, Ministry of Organisation, China, in 2014 and 2016, respectively.

1558-1748 (c) 2018 IEEE. Personal use is permitted, but republication/redistribution requires IEEE permission. See http://www.ieee.org/publications_standards/publications/rights/index.html for more information.